Physics of Fluids ARTICLE scitation.org/journal/phf

Mean-field kinetic theory analysis of vapor flow between evaporating and condensing interfaces in the presence of non-condensable gas molecules

Cite as: Phys. Fluids **33**, 122017 (2021); doi: 10.1063/5.0073118
Submitted: 27 September 2021 · Accepted: 5 December 2021 ·
Published Online: 22 December 2021

Kotaro Ohashi, Kazumichi Kobayashi,[a] Hiroyuki Fujii, and Masao Watanabe

AFFILIATIONS

Division of Mechanical and Space Engineering, Faculty of Engineering, Hokkaido University, Sapporo 060-8628, Japan

[a]Author to whom correspondence should be addressed: kobakazu@eng.hokudai.ac.jp

ABSTRACT

To investigate the vapor kinetic boundary condition (which is the boundary condition for the Boltzmann equation) in the presence of a non-condensable (NC) gas at a non-equilibrium liquid interface, we performed numerical simulations of non-equilibrium vapor (condensable gas) and NC gas mixture flows. The Enskog–Vlasov direct simulation Monte Carlo method (EVDSMC method) was utilized for this two-surface problem to obtain the evaporation and condensation coefficients, which represent the vapor–molecule evaporation and condensation rates, respectively. These coefficients are incorporated in the kinetic boundary condition. The simulation results showed that the evaporation and condensation coefficients decrease with increasing numbers of NC-gas molecules at the liquid interface with the same tendency. To investigate the validity of these coefficients, we also utilized the obtained evaporation and condensation coefficients for Boltzmann equation analysis. Hence, we concluded that these coefficients simply depend on the NC-gas number density at the liquid interface if the liquid temperature is constant. Thus, they are independent of the non-equilibrium or equilibrium state, and therefore, the coefficient values obtained for the equilibrium state can be used in the analysis of a non-equilibrium state. This finding will aid future predictions of non-equilibrium vapor flows with NC gas.

I. INTRODUCTION

Vapor is a condensable gas, and flows of vapor in contact with its condensed phase have been widely studied using molecular gas dynamics (MGD) analysis.[1,2] This approach is required because the non-equilibrium region, called the Knudsen layer, cannot be treated by the Navier–Stokes equation systems.[3,4] Therefore, in the MGD framework, analysis of the Boltzmann equation is essential for vapor flow prediction. To solve this equation, the kinetic boundary condition (KBC) at the vapor–liquid interface is needed.

Several studies concerning vapor flows with non-condensable (NC) gas have been performed using MGD;[5–7] however, few studies on the KBC of vapor with NC gas have been reported. Two parameters are associated with the KBC: the evaporation and condensation coefficients, and many researchers have worked to determine these coefficients for a pure vapor system experimentally,[8] theoretically,[9,10] and using molecular dynamics[11–16] and Enskog–Vlasov equation-based simulations.[17–21] Frezzotti[22] conducted a molecular dynamics simulation for a binary mixture liquid and obtained these coefficients. However, few studies have examined these coefficients in the presence of NC gas. This case is notable because, in many situations, vapor molecules evaporate or condense in the presence of NC gas (e.g., a water–air system).

One of the authors of this paper recently studied the KBC in the presence of NC gas under the vapor/gas–liquid equilibrium state and found that the evaporation and condensation coefficients decrease with increasing NC-gas content in the system.[23,24] However, no studies have investigated the evaporation and condensation coefficients for a vapor–liquid system in a non-equilibrium state with a gas mixture composed of vapor and NC gas. As a practical example of this problem, one of the authors of this paper recently noted that NC gas inside a vapor bubble significantly affects the collapse behavior, i.e., the NC-gas drift at the bubble wall prevents vapor condensation in the final stage of bubble collapse.[25] However, the prevention of vapor condensation remains a hypothesis. Moreover, for droplet evaporation into a gas mixture composed of vapor and NC gas, the KBC for the vapor molecules is needed to predict the precise evaporation mass flux at the interface.[26] To elucidate these processes, we must clarify the values of the evaporation and condensation coefficients at non-equilibrium interfaces.

Here, we explain the evaporation and condensation coefficients α_e^V and α_c^V, respectively. Figure 1(a) shows the molecular mass fluxes of pure vapor across a vapor–liquid interface. As apparent from the figure, we can classify the molecular mass fluxes into five types: J_{out}^V, J_{coll}^V, J_{evap}^V, J_{ref}^V, and J_{cond}^V. Among these molecular mass fluxes, J_{out}^V transitions to the vapor/gas phase from the liquid phase, and J_{coll}^V collides with the liquid phase from the vapor phase. These two fluxes can be decomposed into J_{evap}^V, J_{ref}^V, and J_{cond}^V: J_{evap}^V evaporates into the vapor phase from the liquid phase, J_{ref}^V comes from the vapor phase and is reflected to the vapor phase, and J_{cond}^V condenses into the liquid phase from the vapor phase. These fluxes have the following relationships:

$$J_{\text{out}}^V = J_{\text{evap}}^V + J_{\text{ref}}^V, \quad J_{\text{coll}}^V = J_{\text{cond}}^V + J_{\text{ref}}^V. \tag{1}$$

From the fluxes, α_e^V and α_c^V are defined as follows:[27]

$$\alpha_e^V = \frac{J_{\text{evap}}^V}{J_{\text{out}}^{V*}} = \frac{J_{\text{evap}}^V}{m^V n^{V*}\sqrt{\frac{R^V T_L}{2\pi}}}, \quad \alpha_c^V = \frac{J_{\text{cond}}^V}{J_{\text{coll}}^V}, \tag{2}$$

where the superscript $*$ indicates the equilibrium state, m^V is the mass of a vapor molecule, n^{V*} is the saturated vapor number density, R^V is the gas constant of vapor, and T_L is the liquid temperature. For α_e^V, J_{evap} has been determined to be a function of T_L using the concept of spontaneous evaporation;[12,13] hence, from the definition, α_e^V depends only on T_L in a pure-vapor system. Using these coefficients, the KBC is expressed as follows:

$$f_{\text{out}}^V = \frac{\alpha_e^V n^{V*} + (1-\alpha_c^V) n_{\text{ref}}^V}{(2\pi R^V T_L)^{3/2}} \exp\left(-\frac{\xi_x^2+\xi_y^2+\xi_z^2}{2R^V T_L}\right), \quad (\xi_x > 0), \tag{3}$$

where f_{out}^V is the molecular velocity distribution function (VDF) outgoing from the liquid interface to the vapor phase, and ξ is the vapor–molecule velocity. The subscript x indicates the direction normal to the interface and the y, z subscripts indicate directions tangential to the interface as shown in Fig. 1. Finally, n_{ref}^V is the density of the diffusively reflecting vapor molecules and is expressed by

$$n_{\text{ref}}^V = -\sqrt{\frac{2\pi}{R^V T_L}} \int_{-\infty}^{\infty}\int_{-\infty}^{\infty}\int_{-\infty}^{0} \xi_x f_{\text{coll}}^V \mathrm{d}\xi_x \mathrm{d}\xi_y \mathrm{d}\xi_z, \tag{4}$$

where f_{coll}^V is the molecular velocity distribution function from the vapor phase collision with the liquid phase, and f_{coll}^V is obtained from the analysis of the Boltzmann equation. In summary, the KBC represents the velocity distribution of density $\alpha_e^V n^{V*} + (1-\alpha_c^V) n_{\text{ref}}^V$ specified at T_L for the molecules having the normal velocity leaving from the liquid phase to gas phase.

Regarding KBC at a vapor–liquid interface, various model boundary conditions including general forms have been proposed; Eq. (3) is from the molecular dynamics studies of KBC.[11,12] In this KBC, as shown in Eq. (2), $\alpha_e^V = \alpha_c^V$ is allowed in an equilibrium state where the mass fluxes are obtained as $J_{\text{coll}}^V = J_{\text{out}}^{V*}$ and $J_{\text{evap}}^V = J_{\text{cond}}^V$. However, there is no restriction for these coefficients to be the same value in a non-equilibrium state. Additionally, for strong condensation, the molecular velocity distribution becomes anisotropic and differs from Eq. (3) because the temperature in the VDF deviates from the liquid temperature; the temperatures normal and tangential to the interface are defined, at which molecules transition from liquid to vapor, and they assume different values in the strong condensation state due to the insufficient accommodation of molecules between vapor and liquid molecules.[13,16] However, it has been shown that the Maxwellian with the liquid temperature for the molecules having the normal velocity leaving from the liquid phase to gas phase can be assumed in a weak condensation state.[19] According to this result, we conducted a numerical simulation in a weak non-equilibrium state for Eq. (3) in this study.

Through interaction between the NC-gas molecules and vapor molecules at the interface, as shown in Fig. 1(b), the evaporation/condensation vapor fluxes can decrease, which may cause α_e^V and α_c^V to decrease. In this study, we investigate the evaporation and condensation coefficients for vapor flows in the presence of NC gas using a system of simultaneous evaporating and condensing surfaces known as the two-surface problem. Various non-equilibrium conditions are studied by changing the NC-gas content of the system. Note that a method to construct the KBC for vapor molecules in a single-component system using the Enskog–Vlasov equation based on the two-surface problem was previously proposed by the authors.[19] This study extends this method to the binary mixture problem.

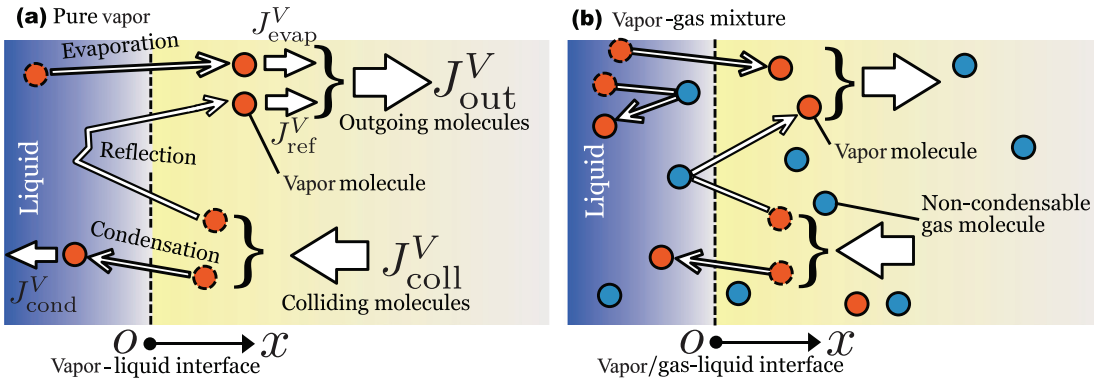

FIG. 1. Schematics of vapor molecular mass fluxes across a vapor/gas–liquid interface: (a) pure vapor system; (b) vapor–gas mixture system. J_{out}^V, J_{coll}^V, J_{evap}^V, J_{ref}^V, and J_{cond}^V are the molecular mass flux outgoing to the vapor/gas phase, a molecular mass flux colliding with the liquid phase, an evaporating molecular mass flux, a reflecting molecular mass flux at the interface, and a condensing molecular mass flux, respectively.

II. SIMULATION METHOD

A. Enskog–Vlasov equation and numerical method

To simulate the vapor/gas-mixture two-surface problem, we focused on the Enskog–Vlasov equation based on the mean-field kinetic theory.[28] This approximate kinetic equation can express the vapor/gas and liquid phase flows. Details of the Enskog–Vlasov equation for a multi-component system are given by Ref. 29. The steady and spatially one-dimensional Enskog–Vlasov equations for vapor and NC gas are as follows:

$$\xi_x \frac{\partial f^V}{\partial x} + \left(\frac{F_x^{VV}}{m^V} + \frac{F_x^{VG}}{m^V}\right)\frac{\partial f^V}{\partial \xi_x} = C_E(f^V, f^V) + C_E(f^V, f^G), \quad (5a)$$

$$\xi_x \frac{\partial f^G}{\partial x} + \left(\frac{F_x^{GG}}{m^G} + \frac{F_x^{GV}}{m^G}\right)\frac{\partial f^G}{\partial \xi_x} = C_E(f^G, f^G) + C_E(f^G, f^V), \quad (5b)$$

where $f^i(x, \boldsymbol{\xi})$ is the VDF, with superscript $i = (V, G)$ denoting vapor (V) or NC gas (G); F_x^{ij} is the attractive mean-field force, with superscript $ij = (VV, VG, GV, GG)$ indicating the vapor–vapor (VV), vapor–NC gas (VG and GV), or NC gas–NC gas (GG) attraction; and C_E is the collision term describing the VDF variation due to molecular collisions.[30] The general spatially three-dimensional and time-dependent form of C_E is available in the literature for a single-component system[17,28,30–32] or a multi-component system.[29] The following is for a binary mixture system:

$$\begin{aligned} C_E(f^i, f^j) = (\sigma^{ij})^2 \int_{-\infty}^{\infty}\int_{-\infty}^{\infty}\int_{-\infty}^{\infty}\int_0^{4\pi} & \\ \times \left\{ Y\left[n\left(\boldsymbol{x} + \frac{\sigma^{ij}}{2}\boldsymbol{k}\right)\right] f^j(\boldsymbol{x} + \sigma^{ij}\boldsymbol{k}, \boldsymbol{\xi}_1^*, t) f^i(\boldsymbol{x}, \boldsymbol{\xi}^*, t) \right. & \\ \left. - Y\left[n\left(\boldsymbol{x} - \frac{\sigma^{ij}}{2}\boldsymbol{k}\right)\right] f^j(\boldsymbol{x} - \sigma^{ij}\boldsymbol{k}, \boldsymbol{\xi}_1, t) f^i(\boldsymbol{x}, \boldsymbol{\xi}, t) \right\} & \\ \times H(\boldsymbol{\xi}_r \cdot \boldsymbol{k})(\boldsymbol{\xi}_r \cdot \boldsymbol{k}) \mathrm{d}^2\boldsymbol{k}\mathrm{d}\boldsymbol{\xi}_1, & \end{aligned} \quad (6)$$

where t is the time, H is the Heaviside step function, and $\boldsymbol{\xi}_r$ is the relative molecular velocity defined by $\boldsymbol{\xi}_r = \boldsymbol{\xi}_1 - \boldsymbol{\xi}$. The post-collision molecular velocities are calculated with the unit vector $\boldsymbol{k}$,

$$\boldsymbol{\xi}^* = \boldsymbol{\xi} + \frac{\mu}{m^i}(\boldsymbol{\xi}_r \cdot \boldsymbol{k})\boldsymbol{k}, \quad (7a)$$

$$\boldsymbol{\xi}_1^* = \boldsymbol{\xi}_1 - \frac{\mu}{m^j}(\boldsymbol{\xi}_r \cdot \boldsymbol{k})\boldsymbol{k}, \quad (7b)$$

$$\mu = \frac{2m^i m^j}{m^i + m^j}. \quad (7c)$$

Y is the pair correlation function, which is a function of the total number density as $Y(n)$. These equations assume that molecules interact with the Sutherland potential,

$$\psi^{ij} = \begin{cases} +\infty, & (r \le \sigma^{ij}), \\ -\phi^{ij}\left(\dfrac{\sigma^{ij}}{r}\right)^{\gamma}, & (r > \sigma^{ij}), \end{cases} \quad (8)$$

where ψ^{ij} is the intermolecular potential between components ij, ϕ^{ij} is the depth of the potential well, r is the distance between two interacting molecules, and γ is a constant related to the depth. In this study, we set $\phi^{VV} = 1.325kT_{\mathrm{cri}}^V$, $\phi^{VG} = \phi^{GV} = 0.364kT_{\mathrm{cri}}^V$, and $\phi^{GG} = 0.1kT_{\mathrm{cri}}^V$. Here, T_{cri}^V is the critical vapor temperature expressed as $T_{\mathrm{cri}}^V = 0.094\,329\frac{4\gamma}{\gamma-3}\frac{\phi^{VV}}{k}$, k is the Boltzmann constant, and $\gamma = 6$. The analysis of evaporation and condensation using this method was mainly performed by studies reported in Refs. 17 and 29 for single or multi-component systems, and their value of ϕ^{VV} was used in this study. They also noted that for this value, molecules behave in the same asymptotic manner as in the 12–6 Lennard-Jones potential. Further, for ϕ^{GG}, the value is set as that of an NC-gas molecule by making the potential well shallow and non-condensing. The relation between the potential wells of ϕ^{VV} and ϕ^{GG} is similar to that of the Xenon and Neon molecules.[32] The value of ϕ^{VG} is determined by the Lorentz–Berthelot rule $\phi^{VG} = \sqrt{\phi^{VV}\phi^{GG}}$. We set the molecular diameter $\sigma = \sigma^{ij}$ and molecular mass $m = m^i$ to the same values for both the vapor and NC-gas molecules to simplify the simulations. In particular, we can use $Y(n) = \frac{1}{2}\frac{2-\eta}{(1-\eta)^3}$, where $\eta = \frac{\pi}{6}n\sigma^3$ under the $\sigma = \sigma^{ij}$ condition. The assumptions $m^G = m^V$ and $\sigma^{GG} = \sigma^{VV}$ are mechanically identical and have been widely used in previous studies of mixture gases (e.g., Refs. 5, 29, and 33). In this study, we focused only on the molecular properties of vapor and NC gas. Thus, the settings in this study are similar to those of the above previous studies. By conducting this study, we investigated the effect that the existence of NC gas itself suppresses the evaporation and condensation of vapor molecules. Thus, the values of ϕ^{VV} and ϕ^{VG} enable us to simulate the vapor and NC gas molecules.[24] NC gas dissolution in the liquid phase occurs in this simulation as shown in Fig. 1. However, the dissolution quantity of NC-gas molecules is extremely low, which leads the evaporation and condensation coefficients of NC-gas molecules, α_e^G and α_c^G, to take the small values of $\alpha_e^G = \alpha_c^G = O(10^{-3})$.[23,24] Further, we can assume the KBC for NC-gas molecules as diffusion reflection. Detailed definitions of α_e^G and α_c^G are given by the above previous studies.

Using the solved equations, we could obtain macroscopic quantities by integrating f^i over the entire velocity space,

$$n^i = \iiint f^i \mathrm{d}\boldsymbol{\xi}, \quad (9a)$$

$$n^i \boldsymbol{v}^i = \iiint \boldsymbol{\xi} f^i \mathrm{d}\boldsymbol{\xi}, \quad (9b)$$

$$\frac{3}{2}n^i k T^i = \frac{1}{2}\iiint m|\boldsymbol{\xi} - \boldsymbol{v}^i|^2 f^i \mathrm{d}\boldsymbol{\xi}, \quad (9c)$$

where $\mathrm{d}\boldsymbol{\xi} = \mathrm{d}\xi_x\mathrm{d}\xi_y\mathrm{d}\xi_z$, $n^i(x)$ is the number density, $\boldsymbol{v}^i(x)$ is the velocity, and $T^i(x)$ is the temperature.

To solve the Enskog–Vlasov equation numerically, we used the Enskog–Vlasov direct simulation Monte Carlo (EVDSMC) method proposed by Refs. 17 and 31. The EVDSMC method is an extension of the direct simulation Monte Carlo (DSMC) method, which is a stochastic particle scheme that solves the Boltzmann equation. The detailed procedure for the EVDSMC method or an overview was presented by Refs. 34 and 35. The EVDSMC method has the following two main advantages: (i) The run time is approximately 100 times less than that for the molecular dynamics simulation when the problem is spatially one-dimensional;[36] (ii) As discussed below, we can distinguish colliding, outgoing, evaporating, reflecting, and condensing molecules using this method.

B. Simulation system

In this section, we explain the simulation system. We focused on the two-surface problem so as to investigate the molecular mass fluxes

at the liquid interface. In this case, the vapor evaporates from a high-temperature liquid and condenses onto a low-temperature liquid, and this problem is the fundamental phenomenon of kinetic theory concerning evaporation and condensation of pure vapor[37,38] or a gas mixture.[5,33,39,40] Addressing this problem with the EVDSMC method allows realization of a steady flow, which is advantageous for adequate sampling of macroscopic quantities.

We used two virtual boundaries at the liquid interface to obtain the molecular mass fluxes: the virtual boundary of the bulk mixture at the gas side, i.e., the gas-mixture boundary, and that at the bulk liquid side, i.e., the liquid boundary. We call this approach the improved interphase boundary method,[14,23] which was improved based on the concept proposed by Refs. 11 and 41. The detailed procedure is presented in Sec. II C.

Figure 2(a) shows a schematic of the simulation system. The high-temperature liquid, with temperature T_L^{high}, was set at the center of the system, and the low-temperature liquid, with temperature T_L^{low}, was set on both sides of the system. NC gas was present between each liquid, and a periodic boundary was assumed at both ends of the system. Various simulation cases were considered in this study, as listed in Table I. By changing the difference in the liquid temperature and NC-gas content of the system, we investigated various non-equilibrium states. We describe the gas-mixture steady flow simulation procedure below.

First, we performed vapor–liquid equilibrium simulations at three different liquid temperatures ($T_L = 0.60T_{\text{cri}}^V$, $0.64T_{\text{cri}}^V$, and $0.68T_{\text{cri}}^V$) to obtain the gas-mixture and liquid boundaries. These temperatures were selected with reference to a previous study.[19] These boundaries were defined by their number density profiles, i.e., the profiles were fitted using the following equation (the 10–90 thickness equation[13]):

$$n^V(x) = \frac{n_{\text{vap}}^V + n_{\text{liq}}^V}{2} \pm \frac{n_{\text{vap}}^V - n_{\text{liq}}^V}{2} \tanh\left(\frac{x - X_m}{0.455\delta}\right), \tag{10}$$

where n_{vap}^V and n_{liq}^V are the number densities of the bulk vapor and liquid phases, respectively; X_m is the density transition-layer center, and δ is its thickness. These relationships are illustrated in Fig. 2(b). For the high- and low-temperature liquids, the signs of the right-hand side were positive and negative for $x > 0$, respectively. Then, the gas-mixture and liquid boundary positions, $x = X_{gb} = X_m \pm 3\delta$ and $x = X_{lb} = X_m \pm \delta$, respectively, were determined. Here, for X_{gb} and X_{lb}, a positive or negative sign denotes the high- or low-temperature liquid at $x > 0$, respectively. The validity of these positions has been discussed previously.[14,42]

Second, we prepared a pure-vapor steady flow using the shift method.[19,43] As initial conditions, a liquid film with temperature T_L^{high} and thickness 20σ was arranged in the system center. On both sides of the system, another liquid film with T_L^{low} and thickness 20σ was arranged. After sufficient time, the vapor flows from the high- to low-temperature liquid films became steady state.

Third, we added sample NC-gas molecules to the pure-vapor steady flow and realized a steady flow for a gas mixture composed of vapor and NC gas. Finally, we sampled the macroscopic quantities in

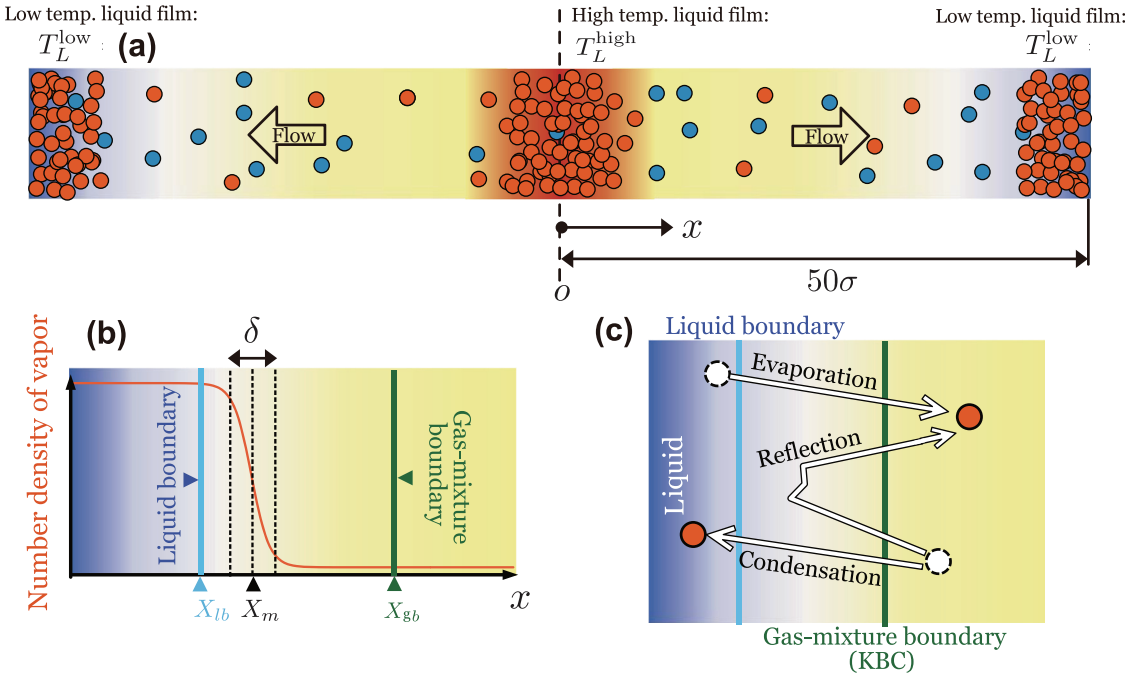

FIG. 2. (a) Present simulation system. A high-temperature liquid film is at the center, a low-temperature liquid film is on each side of the system, and vapor flows from the former to the latter. The system contains NC-gas molecules, and a periodic boundary condition is assumed on both sides of the system. (b) Schematic of vapor density transition layer, where δ and X_m are its thickness and center, respectively, and X_{gb} and X_{lb} are the gas-mixture and liquid boundaries, respectively. (c) Schematic of molecular mass fluxes classified by improved interphase boundary method.

TABLE I. Simulation cases. T_L^{high}/T_{cri}^V and T_L^{low}/T_{cri}^V are the reduced temperatures of the high- and low-temperature liquid films, respectively; N^V is the number of sample vapor molecules in the system, and N^G is the number of sample NC-gas molecules in the system (sample molecules are virtual particles in the DSMC method).

Case no.	T_L^{high}/T_{cri}^V	T_L^{low}/T_{cri}^V	N^V	N^G
1	0.60	0.60	2 500 000	0
2	0.60	0.60	2 500 000	5000
3	0.60	0.60	2 500 000	15 000
4	0.60	0.60	2 500 000	25 000
5	0.60	0.60	2 500 000	50 000
6	0.60	0.60	2 500 000	100 000
7	0.60	0.60	2 500 000	150 000
8	0.60	0.60	2 500 000	250 000
9	0.64	0.60	2 500 000	0
10	0.64	0.60	2 500 000	5000
11	0.64	0.60	2 500 000	15 000
12	0.64	0.60	2 500 000	25 000
13	0.64	0.60	2 500 000	50 000
14	0.64	0.60	2 500 000	100 000
15	0.64	0.60	2 500 000	150 000
16	0.64	0.60	2 500 000	250 000
17	0.68	0.60	2 500 000	0
18	0.68	0.60	2 500 000	5000
19	0.68	0.60	2 500 000	15 000
20	0.68	0.60	2 500 000	25 000
21	0.68	0.60	2 500 000	50 000
22	0.68	0.60	2 500 000	100 000
23	0.68	0.60	2 500 000	150 000
24	0.68	0.60	2 500 000	250 000

the flow field. The sample count was 200 000, and the macroscopic quantities were averaged.

Throughout the simulation, the temperatures of the two-liquid films were controlled.[44] For all simulation cases, we set the cell size $\Delta x = 0.2\sigma$ and the time step $\Delta t = 0.0005\sigma/\sqrt{2RT_{cri}^V}$. The sample-molecule reference number, which corresponds to the critical number density, N_0, was 5000 per cell. In the EVDSMC method, the maximum collision number scheme adopted in the standard DSMC method is used, i.e., the maximum collision number is estimated, and the true collisions are determined stochastically.[31] The post-collision velocities are calculated according to the two-body collision formula as shown in Eq. (7).

C. Method of classifying molecular mass fluxes across a vapor/gas–liquid interface

To determine α_e^V and α_c^V, molecules must be classified. In this study, we used the improved interphase boundary method[14,23] for the molecular mass fluxes. This method assumes two virtual boundaries: the gas-mixture and liquid boundaries, as introduced in Sec. II B. Here, we explain the reasoning behind use of these boundaries.

The gas-mixture boundary position at the liquid surface ($x = X_{gb}$) is considered to impose the KBC. At this position, the vapor is a sufficiently ideal gas; that is, the influence of the intermolecular potential force composed of liquid molecules becomes sufficiently small to be ignored.[24] The pair of gas-mixture and liquid boundary positions obtained for the present condition provides the correct spontaneous evaporating molecular mass flux J_{evap}^V in the vapor–liquid equilibrium and weak non-equilibrium states; that is, using this method, we confirmed the spontaneous evaporation flux in a single-component system in both equilibrium and weak non-equilibrium states. Additionally, we showed that J_{evap}^V has the same value in the equilibrium and non-equilibrium states[14,42] and can be obtained as a function of the liquid temperature,[45] which is the same concept as of spontaneous evaporation.[12]

Using the two boundaries, we can classify and obtain each flux value as follows [Fig. 2(c)]: (i) J_{cond}^V is determined when the vapor molecule crosses the gas-mixture boundary and then the liquid boundary; (ii) J_{ref}^V is determined when the vapor molecule crosses the gas-mixture boundary and then passes it for a second time; and (iii) J_{evap}^V is determined when the vapor molecule crosses the liquid boundary and then the gas-mixture boundary. These values are defined by

$$J = \frac{mN}{S\Delta t}, \tag{11}$$

where N is the number of sample molecules given by each trajectory stated above, and S is the system cross section. In Sec. III, we present the results of the simulations described in this section.

D. Equilibrium properties

Next, we show the results of vapor/gas–liquid equilibrium simulations (Cases 1–8). Figure 3 shows the result of Case 8, which is the typical equilibrium case for vapor/gas–liquid coexistence. As shown in Fig. 3, the liquid phase was formed in the left side, and the vapor/gas phase was formed in the right side. The profiles of the mean-field force for the vapor and NC gas, $F_x^V = F_x^{VV} + F_x^{VG}$ and $F_x^G = F_x^{GG} + F_x^{GV}$, are also plotted in Fig. 3. We can confirm that the absolute value of F_x^V is larger than that of F_x^G: vapor molecules can form the liquid phase owing to these forces. We also confirmed that the force profiles were

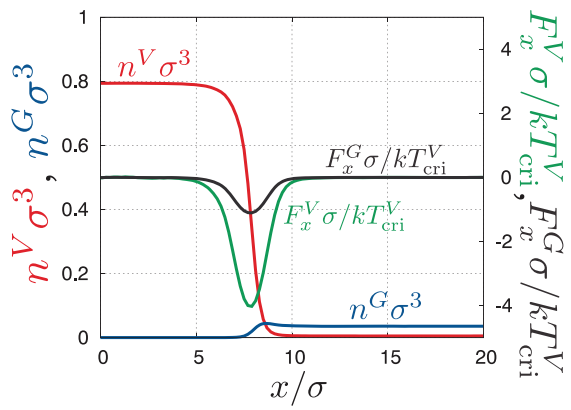

FIG. 3. Vapor/gas–liquid equilibrium state of Case 8: non-dimensional vapor number density, $n^V\sigma^3$; non-dimensional NC-gas number density, $n^G\sigma^3$; non-dimensional vapor mean-field force, $F_x^V\sigma/kT_{cri}^V$; and non-dimensional NC-gas mean-field force, $F_x^G\sigma/kT_{cri}^V$.

not so different for Cases 1–8 because the liquid densities were almost constant.

The detailed data of Cases 1–8 are listed in Table II. In Table II, $n^V_{\rm liq}$, $n^V_{\rm vap}$, $n^G_{\rm liq}$, and $n^G_{\rm gas}$ are the non-dimensional bulk number densities of the vapor molecules in the liquid phase, vapor molecules in the vapor/gas phase, NC-gas molecules in the liquid phase, and NC-gas molecules in the vapor/gas phase, respectively. Further, $c^V_{\rm vap}$ is the concentration of the vapor in the vapor/gas phase calculated as $c^V_{\rm vap} = n^V_{\rm vap}/(n^V_{\rm vap} + n^G_{\rm gas})$. The compression factor Z, indicating a deviation from the ideal gas state, is calculated as

$$Z = p/n^V_{\rm vap} kT, \tag{12}$$

where $p(n, T, c^V)$ is the pressure. This pressure is obtained using the following van der Waals equation of state:[29]

$$p = nkT\frac{(1+\eta+\eta^2-\eta^3)}{(1-\eta)^3} - \frac{2}{3}\pi\frac{\gamma}{(\gamma-3)}\sigma^3 n^2\left[c^V\phi^{VV} + 2c^V(1-c^V)\phi^{VG} + (1-c^V)^2\phi^{GG}\right]. \tag{13}$$

The above equation of state can be applied to both vapor/gas–liquid phases. Now, to obtain Z, we used $p(n = n^V_{\rm vap} + n^G_{\rm gas}, T = 0.60T^V_{\rm cri}, c^V = c^V_{\rm vap})$, which is the total pressure in the vapor/gas phase specified at the temperature $T = 0.60T^V_{\rm cri}$. λ^{VV} and λ^{VG} are the mean free paths of vapor (or NC gas) molecules with respect to the vapor and NC gas molecules defined as

$$\lambda^{VV}/\sigma = 1/\left(\sqrt{2}\pi n^V_{\rm vap}\sigma^3\right), \quad \lambda^{VG}/\sigma = 1/\left(\sqrt{2}\pi n^G_{\rm gas}\sigma^3\right). \tag{14}$$

From Table II, as the case number increases, that is, as NC-gas content increases in the vapor/gas phase, $c^V_{\rm vap}$ decreases. However, the values of Z were almost unity for all cases; the mixture gas can be treated as an ideal gas. λ^{VV} was almost unchanged because $n^V_{\rm vap}$ was constant, while λ^{VG} decreased with the increase in the NC gas content.

III. RESULTS AND DISCUSSION

A. Macroscopic quantities

We present the flow-field macroscopic quantities determined from the simulation results. Note that analyses with similar systems were conducted in previous studies[33,39,40] using the Boltzmann equation analysis with the KBCs; in many cases, the complete condensation condition, $\alpha^V_e = \alpha^V_c = 1$, was used for the KBC of vapor molecules, and the diffusion reflection condition, $\alpha^G_e = \alpha^G_c = 0$, was used for NC-gas molecules. Figure 4 shows the macroscopic quantities for Cases 17 (pure vapor) and 21 (gas mixture), which are typical flow-field examples. Figure 4(a) shows the overall density of the pure vapor (Case 17). A high-temperature liquid film ($T^{\rm high}_L = 0.68T^V_{\rm cri}$) formed at the center of the simulation system, whereas a low-temperature liquid film ($T^{\rm low}_L = 0.60T^V_{\rm cri}$) formed at the left and right sides. The vapor flow occurred between these liquid films. Because the system is symmetrical, we show a spatial range of $[0\sigma, 50\sigma]$ hereafter. The gas-mixture boundaries (the positions at which the KBC is imposed) determined by the method described above (Sec. II B) are also shown in Fig. 4(a). The region inside the boundaries can be treated using the Boltzmann equation.

Figure 4(b) shows the non-dimensional number densities. The number densities of the pure vapor and the vapor component of the gas mixture were lower along the flow direction. In contrast, that of the NC gas was higher, as the NC gas was swept by the vapor flow. This tendency is the same as that given by the DSMC results of Ref. 33.

Figure 4(c) shows the non-dimensional temperature distributions. In the pure-vapor case, we observed an inverted temperature gradient due to evaporation/condensation in the gas phase. Similar results have been observed in previous MD simulations;[43] the temperature gradient becomes positive from the high-temperature liquid to the low-temperature liquid in the gas phase. When NC gas was added to the system, the vapor temperature gradient weakened. We confirmed a regular gradient in the weak evaporation/condensation system.

Figures 4(d) and 4(e) show the non-dimensional velocities and mass fluxes normal to the interface, respectively. We stress that the vapor mass fluxes were spatially uniform (inside the boundaries); hence, the system reached a steady state because of mass conservation. For both the velocities and mass fluxes, the vapor component of the gas mixture decreased in the presence of NC gas compared to that in the pure-vapor case.[39,40] The NC-gas velocity and mass flux were zero over the region, which means that the NC gas was completely at rest. This result is identical to the results of previous studies and is explained as follows:[5,33] (i) the NC gas neither evaporates nor condenses at the two interfaces and hence, $n^G v^G_x = 0$ at the interfaces; (ii)

TABLE II. Vapor–gas/liquid coexistence data of Cases 1-8 (equilibrium simulations).

Case no.	$n^V_{\rm liq}\sigma^3$	$n^V_{\rm vap}\sigma^3$	$n^G_{\rm liq}\sigma^3$	$n^G_{\rm gas}\sigma^3$	$c^V_{\rm vap}$	Z	λ^{VV}/σ	λ^{VG}/σ
1	0.791	0.004 97	0.000 00	0.000 00	1.00	0.96	45.3	···
2	0.792	0.004 98	0.000 00	0.000 72	0.87	0.97	45.2	310.6
3	0.791	0.005 00	0.000 01	0.002 11	0.70	0.97	45.1	106.5
4	0.791	0.005 01	0.000 02	0.003 55	0.59	0.98	45.0	63.4
5	0.792	0.005 06	0.000 03	0.007 08	0.42	0.99	44.5	31.8
6	0.792	0.005 14	0.000 04	0.014 20	0.27	1.00	43.8	15.8
7	0.793	0.005 22	0.000 09	0.021 41	0.20	1.01	43.0	10.5
8	0.794	0.005 40	0.000 16	0.035 57	0.13	1.04	41.8	6.3

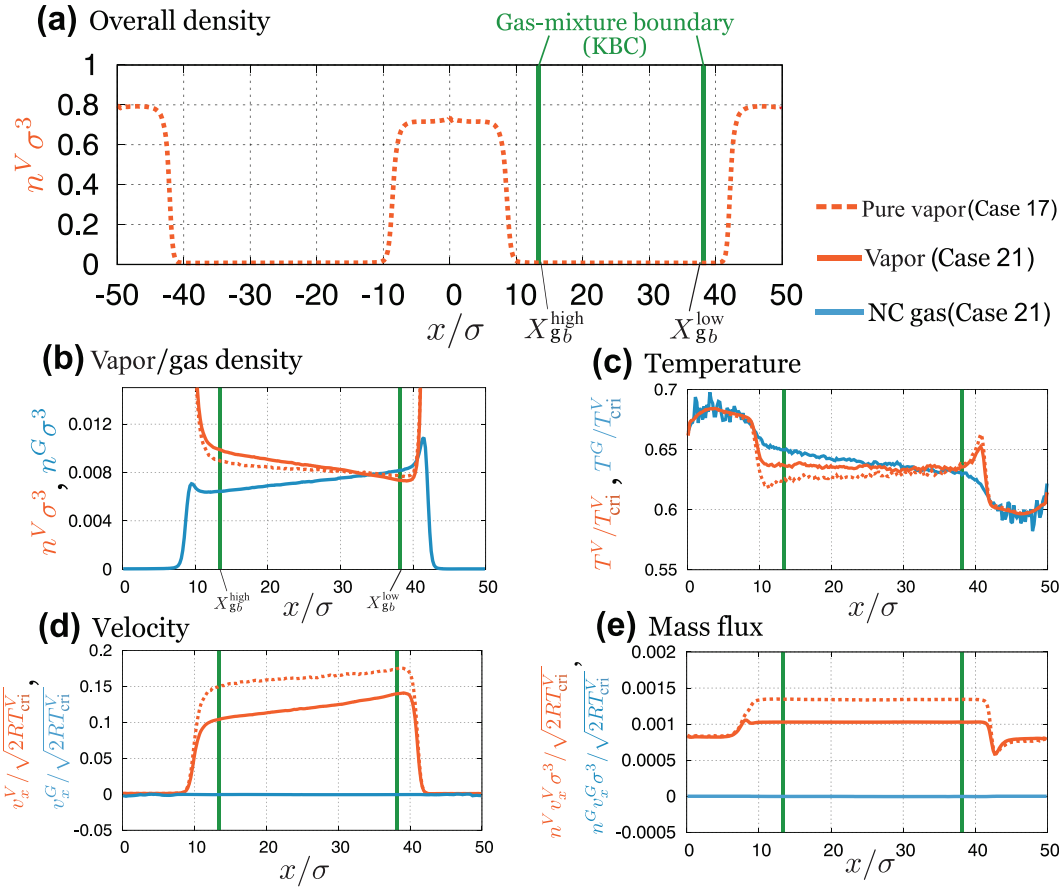

FIG. 4. Flow-field macroscopic quantities. The red dotted line represents Case 17 (pure vapor), whereas the red and blue solid lines represent the Case-21(gas mixture) vapor and NC-gas components, respectively: (a) non-dimensional number density (overall region), $n^V\sigma^3$; (b) non-dimensional number density (vapor/gas region), $n^V\sigma^3$ and $n^G\sigma^3$; (c) non-dimensional temperature distribution, $T^V/T^V_{\rm cri}$ and $T^G/T^V_{\rm cri}$; (d) non-dimensional velocity, $v^V_x/\sqrt{2RT^V_{\rm cri}}$ and $v^G_x/\sqrt{2RT^V_{\rm cri}}$; and (e) non-dimensional mass flux, $n^Vv^V_x\sigma^3/\sqrt{2RT^V_{\rm cri}}$ and $n^Gv^G_x\sigma^3/\sqrt{2RT^V_{\rm cri}}$.

when the system is in the steady state, the mass flux is spatially uniform because of mass conservation. These two conditions yield $n^Gv^G_x = 0 (v^G_x = 0)$ throughout the system. From these results, we confirmed that the EVDSMC simulations were consistent with the results of previous studies.[33,39,40,43]

The vapor properties due to evaporation/condensation for all simulation cases are shown in Fig. 5. We defined the liquid temperature difference as

$$\Delta T_L = T_L^{\rm high} - T_L^{\rm low}. \tag{15}$$

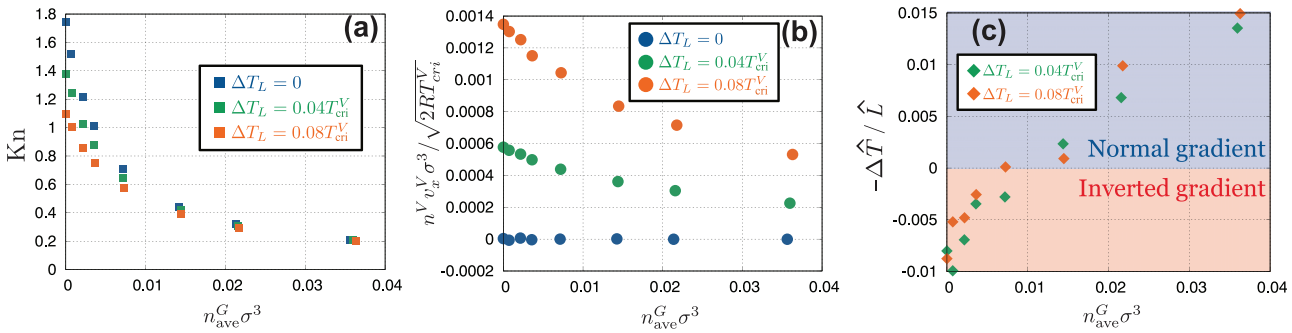

FIG. 5. (a) Knudsen number, (b) vapor mass flux, and (c) temperature gradient for all simulations as functions of average NC-gas number density in gas phase, $n^G_{\rm ave}$.

We also introduced the average NC-gas number density, n^G_{ave}, in the gas phase to organize the results.

Figure 5(a) shows the Knudsen number[2] in the gas phase for the entire simulation, where the Knudsen number is defined as follows:

$$\text{Kn} = \frac{\lambda}{L} = \frac{1/\left[\sqrt{2}\pi\sigma^2(n^V_{\text{ave}} + n^G_{\text{ave}})\right]}{X^{\text{low}}_{gb} - X^{\text{high}}_{gb}}. \tag{16}$$

Here, n^G_{ave} is the average number density of the vapor molecules; X^{high}_{gb} and X^{low}_{gb} are the gas-mixture boundary positions (imposed KBC position) at the high- and low-temperature liquid interfaces, respectively; L is the gas-region system length, defined as $L = X^{\text{low}}_{gb} - X^{\text{high}}_{gb}$; and λ is the mean free path in the gas phase. As shown in the figure, when the average NC-gas number density increased, the Knudsen number decreased due to the decrease in the mean free path in the gas region.

Figure 5(b) shows the vapor mass fluxes in the gas phase, $n^V v^V_x$, due to evaporation and condensation at the liquid surfaces in this simulation. The following two trends are apparent: (i) a higher liquid temperature difference increased the vapor mass fluxes; (ii) the vapor mass fluxes decreased with the average NC-gas number density in the vapor/gas region. From these results, we can confirm that the liquid temperature difference causes the mass flux as a result of evaporation/condensation in the gas phase, and the presence of NC-gas molecules decreases the mass flux.

Figure 5(c) shows the gas-phase temperature. We defined this temperature gradient using the temperatures at the evaporating and condensing liquid surfaces at $x = X^{\text{high}}_{gb}$ and $x = X^{\text{low}}_{gb}$, as follows:

$$-\frac{\Delta\hat{T}}{\hat{L}} = \frac{\left[T^V(X^{\text{high}}_{gb}) - T^V(X^{\text{low}}_{gb})\right]\sigma}{\Delta T L} = \frac{\left[T^V(X^{\text{high}}_{gb}) - T^V(X^{\text{low}}_{gb})\right]\sigma}{(T^{\text{high}}_L - T^{\text{low}}_L)(X^{\text{low}}_{gb} - X^{\text{high}}_{gb})}. \tag{17}$$

As shown in the figure, for small n^G_{ave}, i.e., large Knudsen number cases, an inverted temperature gradient was observed in the gas phase. However, when the normalized n^G_{ave} exceeded approximately 0.01, the temperature gradient became normal because the evaporation and condensation were weakened by the presence of NC-gas molecules, as shown in Fig. 5(b).

Next, we obtained the classified values of the molecular mass fluxes (J^V_{coll}, J^V_{evap}, and J^V_{cond}) to determine α^V_e and α^V_c using the improved interphase boundary method.

B. Molecular mass fluxes and evaporation/condensation coefficients

First, α^V_e and α^V_c, which are significant parameters for the KBC, were determined at the condensing liquid surface. The condensing surface was considered because the influence of the NC-gas molecules on the phase change is easily observed at that location, as the NC-gas molecule drift is enhanced at the condensing surface. The number density ratio of the NC gas to vapor at the position where the gas-mixture boundary was imposed is defined by

$$\hat{n}^{G/V*} = \frac{n^G}{n^{V*}_p(T^{\text{low}}_L)}, \quad T^{\text{low}}_L = 0.60T^V_{\text{cri}}, \tag{18}$$

where n^G is obtained at the gas-mixture boundary at the condensing surface ($x = X^{\text{low}}_{mb}$), and $n^{V*}_p(T^{\text{low}}_L)$ is the saturated vapor number density in the pure vapor system. Note that $n^{V*}_p(T^{\text{low}}_L)$ is constant if the liquid temperature is constant.

Figure 6(a) shows the non-dimensional saturated vapor number density $n^{V*}\sigma^3$ at T^{low}_L obtained using the results of Cases 1–8 (the equilibrium simulations). These values are needed to calculate the denominator of α^V_e from Eq. (2). From the figure, these densities increased linearly with $\hat{n}^{G/V*}$ and could be fitted by

$$n^{V*}\sigma^3 = 0.000\,059\,1\hat{n}^{G/V*} + 0.004\,97, \quad \mathscr{R}^2 = 0.999, \tag{19}$$

where $\mathscr{R}^2$ is the coefficient of determination. The increase in the saturated vapor density was caused by dissolution of the NC-gas molecules into the liquid. The increase trend was determined by ψ^{VG}, that is, the dissolution of the NC-gas molecules in the liquid phase increased the saturated number density of the vapor molecules.

Before we present the vapor molecular mass fluxes, we illustrate the relationship between the gas-mixture flow and molecular fluxes. Figure 6(b) shows a schematic of the flow field and J^V_{coll}, J^V_{cond}, and J^V_{evap}. These fluxes are needed to calculate α^V_e and α^V_c. In the considered system, the vapor flowed to the condensing surface. The vapor flow had the same direction as J^V_{coll}, i.e., across the gas-mixture boundary. Further, J^V_{cond}, which is a component of J^V_{coll} and passed from the gas-mixture boundary to the liquid boundary, was also in the same direction. However, J^V_{evap} was oriented opposite to the vapor flow. Additionally, a high-density layer of NC-gas molecules existed between the gas-mixture and liquid boundaries swept by the vapor flows. Consequently, the values of these fluxes were affected by not only the evaporation- and condensation-driven vapor flow but also the NC-gas content adjacent to the condensing surface, which is represented by $\hat{n}^{G/V*}$.

Figures 6(c) and 6(d) show the non-dimensional molecular mass fluxes $\hat{J}^{V*}_{\text{out}}$, $\hat{J}^V_{\text{evap}}$, $\hat{J}^V_{\text{coll}}$, and $\hat{J}^V_{\text{cond}}$. Here, $\hat{J}^{V*}_{\text{out}} = n^{V*}\sigma^3\sqrt{\frac{T^{\text{low}}_L}{4\pi T^V_{\text{cri}}}}$ was calculated using Eq. (19). When $\hat{n}^{G/V*}$ was equal to zero (pure vapor), $\hat{J}^V_{\text{evap}}$ was almost constant despite differences in ΔT_L. It is emphasized that spontaneous evaporation mass flux, for which $\hat{J}^V_{\text{evap}}$ is constant if the liquid temperature is constant, was observed in the non-equilibrium liquid surface using the improved interphase method. As $\hat{n}^{G/V*}$ increased, $\hat{J}^V_{\text{evap}}$ was suppressed. We consider that the NC-gas molecules between the gas-mixture and liquid boundaries prevent evaporation of the vapor molecules. In contrast to $\hat{J}^V_{\text{evap}}$, when $\hat{n}^{G/V*} = 0$, $\hat{J}^V_{\text{coll}}$ and $\hat{J}^V_{\text{cond}}$ increased in accordance with ΔT_L, as these fluxes are enhanced by vapor flows. Increased $\hat{n}^{G/V*}$ yielded decreased $\hat{J}^V_{\text{coll}}$ and $\hat{J}^V_{\text{cond}}$ (non-equilibrium cases, i.e., $\Delta T_L = 0.04T^V_{\text{cri}}$ and $0.08T^V_{\text{cri}}$). The decrease in $\hat{J}^V_{\text{cond}}$ relative to $\hat{J}^V_{\text{coll}}$ was remarkable. For the same reason as above, we consider that the NC-gas molecules between the gas-mixture and liquid boundaries prevent condensation of the vapor molecules. However, the equilibrium state ($\Delta T_L = 0$) is an exception, as $\hat{J}^{V*}_{\text{coll}} (= \hat{J}^{V*}_{\text{out}})$ increases with increased NC-gas content.[23,24]

We calculated α^V_e and α^V_c from the molecular mass fluxes reported above using Eq. (2); the results are shown in Figs. 6(e) and 6(f). These coefficients decreased linearly with increased NC-gas

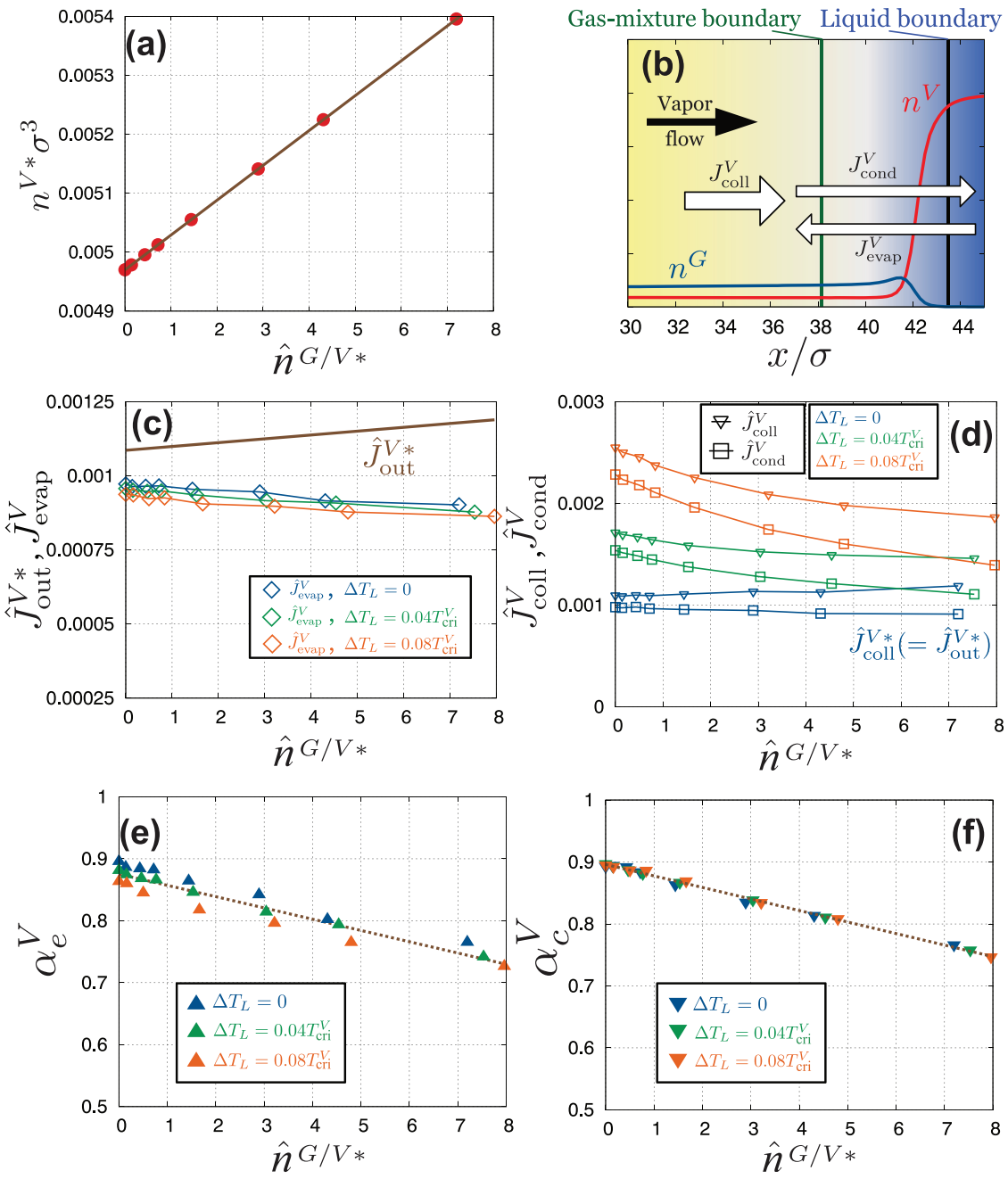

FIG. 6. Molecular mass fluxes at condensing interface ($T_L^{\rm low} = 0.60T^V_{\rm cri}$) and evaporation, α^V_e, and condensation, α^V_c, coefficients organized by $\hat{n}^{G/V}$ under non-equilibrium (including equilibrium) conditions: (a) non-dimensional saturated vapor number density, $n^{V*}\sigma^3$; (b) schematic relationship between vapor flow and molecular mass fluxes $J^V_{\rm coll}$, $J^V_{\rm cond}$, and $J^V_{\rm evap}$; (c) $J^{V*}_{\rm out}$ and $J^V_{\rm evap}$; (d) $J^V_{\rm coll}$ and $J^V_{\rm cond}$; (e) α^V_e; and (f) α^V_c.

content for both the non-equilibrium and equilibrium states, despite the differences in the molecular mass fluxes shown in Figs. 6(c) and 6(d). From these figures, we can also confirm that these coefficients have the same decreasing trend; thus, we can regard $\alpha^V_e = \alpha^V_c$ as a function of $\hat{n}^{G/V*}$.

The suppression of both the vapor evaporation and condensation was caused by molecular reflection at the surface. The vapor molecule reflection originated from the molecular collisions between the vapor and NC gas. Further, according to Bird, the molecular collision number is directly proportional to the number density.[46] Therefore, we

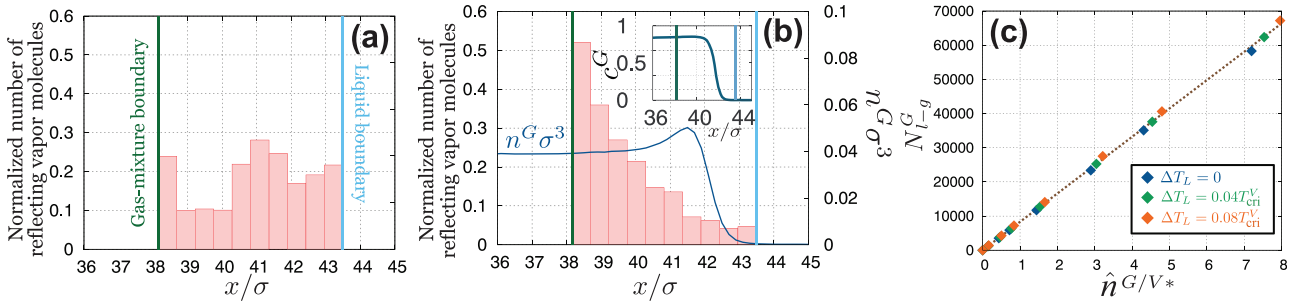

FIG. 7. Reflecting position distribution of vapor molecules at the condensing liquid interface ($T_L^{low} = 0.60T_{cri}^V$) inside the gas mixture and liquid boundaries: (a) Case 1 (pure vapor, equilibrium state); (b) Case 24 (vapor–gas mixture, non-equilibrium state); and (c) total number of NC-gas molecules, N^G_{l-g}, between liquid and gas-mixture boundaries as a function of $\hat{n}^{G/V*}$. The inset of (b) shows the NC-gas concentration profile.

assume that these coefficients are functions of the NC-gas number densities. In this study, we investigated the reflecting position of the vapor molecules and considered the influence of the NC-gas molecules on the vapor molecule reflection.

Figures 7(a) and 7(b) show the reflecting position distribution of the vapor molecules. The red bar graph indicates the number of reflecting molecules at each position; the sum of the graph is normalized to unity. The reflecting position is defined as the maximum vapor–molecule reach position between the gas-mixture and liquid boundaries.[14] Figure 7(a) shows the Case-1 results (pure-vapor and equilibrium case). From the figure, the vapor molecules were reflected between gas-mixture and liquid boundaries relatively uniformly. Figure 7(b) shows the Case-24 result (highest NC-gas content and non-equilibrium case). In contrast to the pure-vapor case, a clear difference in reflecting position distribution was observed; thus, the vapor molecules tended to be reflected at the gas-mixture boundaries because of the NC gas presence. We regard this reflection as being due to the number of NC-gas molecules. Figure 7(c) shows the total number of NC-gas molecules between the gas-mixture and liquid boundaries, N^G_{l-g}, for all simulations. From the figure, the total number of NC-gas molecules was proportional to the NC-gas-molecule number density at the gas-mixture boundary. As a result of the linear increase in the total number of NC-gas molecules, vapor–molecule condensation or evaporation was prevented at the interface. Consequently, the evaporation/condensation coefficients decreased. These results and considerations imply that the NC-gas content at the condensing surface itself directly decreases the evaporating/condensing molecular mass fluxes.

Figures 8(a) and 8(b) show the evaporation and condensation coefficients at the high-temperature liquid. The abscissa indicates the number density ratio at the high-temperature liquid interface, $\hat{n}^{G/V*} = n^G/n_p^{V*}(T_L^{high})$, and the ordinate indicates the normalized evaporation and condensation coefficients, $\alpha_e^V/\alpha_{e,p}^V$ and $\alpha_c^V/\alpha_{c,p}^V$, where $\alpha_{e,p}^V$ and $\alpha_{c,p}^V$ are the evaporation and condensation coefficients for the pure-vapor case, respectively. From the previous study, these coefficients are functions of the liquid temperature for the pure-vapor case. As the temperature increases, these coefficients decrease. From the figures, these coefficients decreased linearly with increased $\hat{n}^{G/V*}$, for the same reason as that at the low-temperature liquid interface. Furthermore, α_e^V had the same decrease tendency as α_c^V, and $\alpha_e^V/\alpha_{e,p}^V \approx \alpha_c^V/\alpha_{c,p}^V$ as a function of $\hat{n}^{G/V*}$ for each liquid temperature.

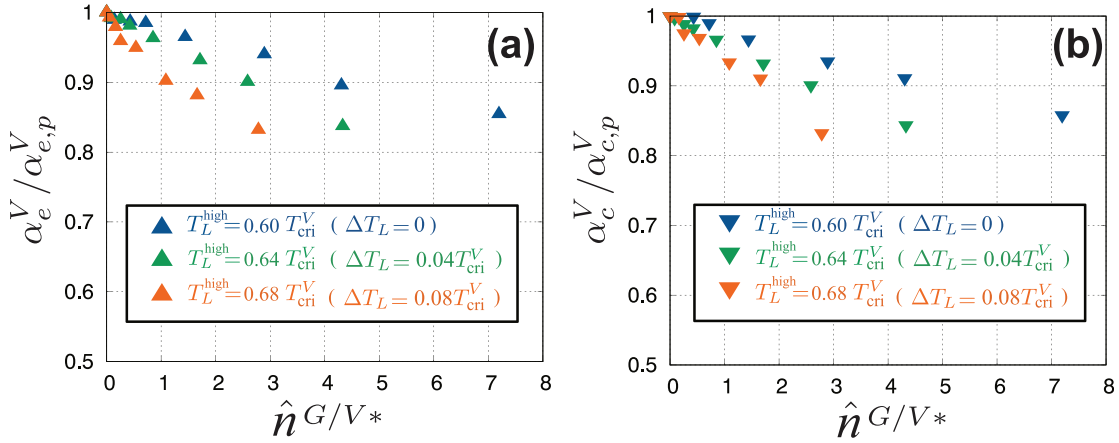

FIG. 8. Evaporation and condensation coefficients at the high-temperature liquid interface as functions of $\hat{n}^{G/V*}$: (a) α_e^V normalized by $\alpha_{e,p}^V$ at $T_L^{high} = 0.60T_{cri}^V$, $0.64T_{cri}^V$, and $0.68T_{cri}^V$, where $\alpha_{e,p}^V$ is the evaporation coefficient in the pure-vapor case; and (b) α_c^V normalized by $\alpha_{c,p}^V$ at $T_L^{high} = 0.60T_{cri}^V$, $0.64T_{cri}^V$, and $0.68T_{cri}^V$, where $\alpha_{c,p}^V$ is the condensation coefficient in the pure-vapor case.

IV. APPLICATION TO BOLTZMANN EQUATION ANALYSIS

The values of α_e^V and α_c^V obtained from the Enskog–Vlasov equation were applied to analysis of the Boltzmann equation, and the coefficient values reported in Sec. III were validated. As reported above, these coefficients depend only on the NC-gas content at the interface regardless of the equilibrium or non-equilibrium state. Hence, we can apply the equilibrium state values, which are easy to obtain, to the two-surface problem described by the Boltzmann equation. The DSMC method was employed as the numerical method for analysis of the Boltzmann equation, and the results were compared with those of the EVDSMC method. Using the Knudsen number, the total number of NC-gas molecules, and the saturated vapor number densities at T_L^{high} and T_L^{low} obtained from the Enskog–Vlasov equation, we performed the DSMC simulation.

From the EVDSMC simulations, we confirmed that the VDF is Maxwellian at the liquid temperature. Reference 19 has shown that VDF becomes Maxwellian for weak evaporation/condensation; the non-equilibrium degree did not exceed the previous simulation conditions. Hence, we could use Eq. (2) for the high- or low-temperature liquid interfaces as the KBC of vapor, as follows:

$$f_{\text{out}}^V(X_{gb}^{\text{high}}) = \frac{\alpha^V n^{V*} + (1-\alpha^V) n_{\text{ref}}^V}{(2\pi R T_L^{\text{high}})^{3/2}} \exp\left(-\frac{\xi_x^2+\xi_y^2+\xi_z^2}{2RT_L^{\text{high}}}\right), \quad (\xi_x > 0), \tag{20a}$$

$$f_{\text{out}}^V(X_{gb}^{\text{low}}) = \frac{\alpha^V n^{V*} + (1-\alpha^V) n_{\text{ref}}^V}{(2\pi R T_L^{\text{low}})^{3/2}} \exp\left(-\frac{\xi_x^2+\xi_y^2+\xi_z^2}{2RT_L^{\text{low}}}\right), \quad (\xi_x < 0), \tag{20b}$$

where we assumed $\alpha^V = \alpha_e^V = \alpha_c^V$, which is a function of $\hat{n}^{G/V*}$. For the NC-gas molecules, we utilized the diffusion reflection condition, as follows:

$$f_{\text{out}}^G(X_{gb}^{\text{high}}) = \frac{n_{\text{ref}}^G}{(2\pi R T_L^{\text{high}})^{3/2}} \exp\left(-\frac{\xi_x^2+\xi_y^2+\xi_z^2}{2RT_L^{\text{high}}}\right), \quad (\xi_x > 0), \tag{21a}$$

$$f_{\text{out}}^G(X_{gb}^{\text{low}}) = \frac{n_{\text{ref}}^G}{(2\pi R T_L^{\text{low}})^{3/2}} \exp\left(-\frac{\xi_x^2+\xi_y^2+\xi_z^2}{2RT_L^{\text{low}}}\right), \quad (\xi_x < 0), \tag{21b}$$

where n_{ref}^G was obtained from Eq. (4) for NC-gas molecules. The hard-sphere molecule model and maximum collision number scheme were adopted. Using the above KBCs and settings, simulations based on the DSMC method were conducted.

Figure 9(a) shows the α_e^V and α_c^V at each liquid temperature obtained from the equilibrium simulations with the EVDSMC method, as shown in Figs. 6(e) and 6(f). These coefficients are linear functions of $\hat{n}^{G/V*}$ for each liquid temperature. Hence, we could obtain the value of $\alpha^V (= \alpha_e^V = \alpha_c^V)$ as a function of $\hat{n}^{G/V*}$ in Eq. (20). α^V is expressed as follows:

$$\alpha^V(T_L, \hat{n}^{G/V*}) = A\hat{n}^{G/V*} + B, \tag{22}$$

where the values of $A(T_L)$ and $B(T_L)$ are constant: $A = -0.0184$ and $B = 0.893$ for $T_L = 0.60T_{\text{cri}}^V$; $A = -0.0306$ and $B = 0.848$ for $T_L = 0.64T_{\text{cri}}^V$; and $A = -0.0429$ and $B = 0.786$ for $T_L = 0.68T_{\text{cri}}^V$, respectively.

In Figs. 9(b)–9(d), the results of the Boltzmann equation are compared with those of the Enskog–Vlasov equation (EVDSMC method) for the number density, velocity normal to the interface, and temperature fields of Cases 10 and 21. Note that a new spatial coordinate system defined by $\chi = (x - X_{gb}^{\text{high}})/(X_{gb}^{\text{low}} - X_{gb}^{\text{high}})$ was introduced. In this coordinate system, $\chi = 0$ and $= 1$ correspond to the evaporating and condensing liquid surfaces, respectively. For Case 10, α^V values were 0.845 and 0.890 at the high- and low-temperature liquids, respectively; for Case 21, α^V values were 0.763 and 0.863 at the high- and low-temperature liquids, respectively, as obtained from Fig. 9(a). From the figures, the values are almost identical to those of the EVDSMC method for vapor and NC gas.

These results imply that even the α_e^V and α_c^V values calculated in the equilibrium state are sufficient for the non-equilibrium vapor flow described by the Boltzmann equation. This is because the coefficient values simply depend on the NC-gas content at the vapor/gas–liquid interface in a weak non-equilibrium state. This finding has practical implications for simulations of various non-equilibrium gas-mixture flows composed of vapor and NC-gas molecules; that is, it may be possible to simulate non-equilibrium gas-mixture flows using α_e^V and α_c^V determined under equilibrium conditions.

V. CONCLUSION

To investigate the evaporation and condensation coefficients incorporated in the vapor KBC, the two-surface problem involving a binary mixture system composed of vapor molecules and NC-gas molecules was simulated using the Enskog–Vlasov equations. The EVDSMC method was used as a numerical method. The improved interphase boundary method was also used to classify molecules for molecular mass fluxes, which were needed to obtain the evaporation and condensation coefficients. We mainly focused on the condensing liquid surface, because the NC gas remarkably influences the coefficients at the condensing surface.

The simulation results showed that the macroscopic flow field given by the EVDSMC method is consistent with those of previous studies. Furthermore, the evaporation and condensation coefficients were calculated for various combinations of non-equilibrium (including equilibrium) conditions and NC-gas contents. We found that these coefficients simply depend on the NC-gas number density at the vapor/gas–liquid interface, regardless of the equilibrium or non-equilibrium state. Specifically, the coefficients decrease linearly with respect to the NC-gas number density. We also found that the number of NC-gas molecules adjacent to the liquid interface is directly related to decreases in the evaporation and condensation coefficients, which implies that collisions between the vapor molecules and NC-gas molecules cause a decrease in the evaporation or condensation molecular mass flux. Finally, we applied the vapor evaporation and condensation coefficients under equilibrium conditions to the KBC for the Boltzmann equation and verified the values of these coefficients.

From these results, we conclude that the vapor evaporation and condensation coefficients can be estimated using the coefficient values of the equilibrium state, and that these values can be applied to a non-equilibrium state. This is a useful and practical finding regarding prediction of non-equilibrium vapor flows with NC gas. In the present simulation, we utilized simple vapor and NC-gas molecules for

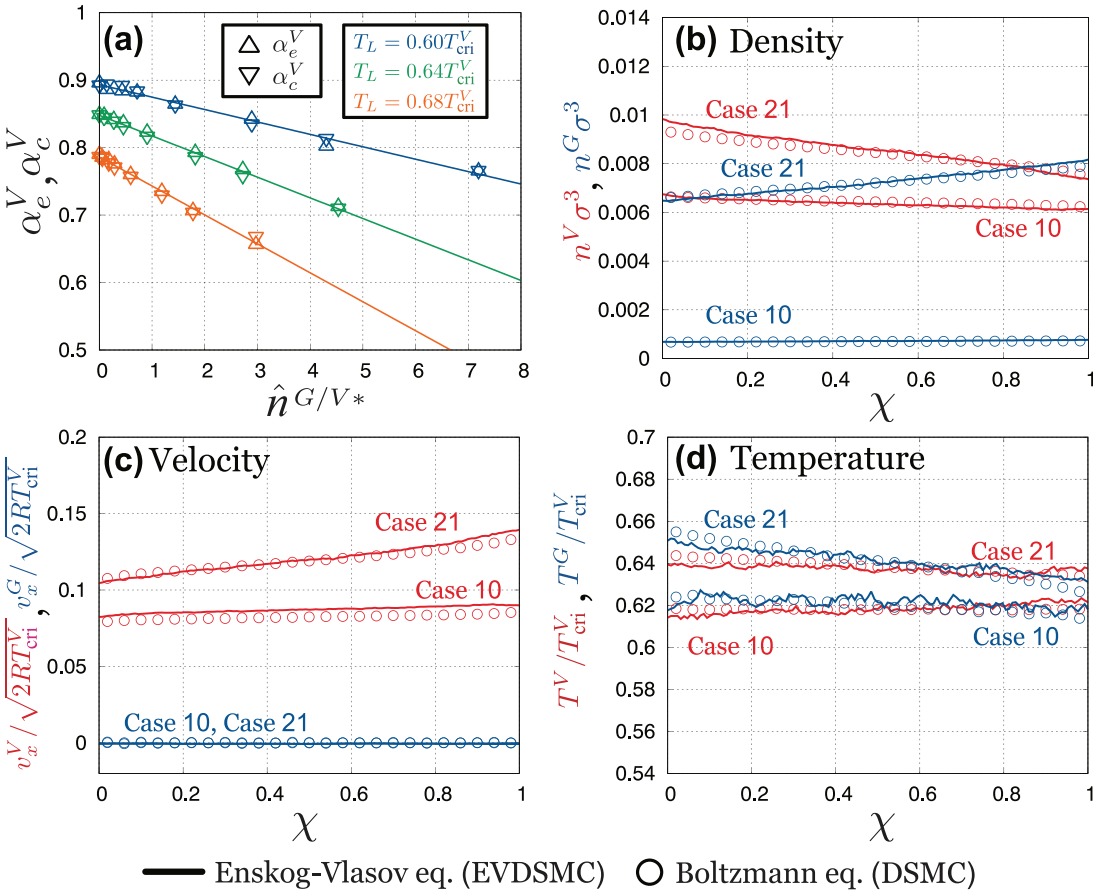

FIG. 9. (a) Evaporation and condensation coefficients in each equilibrium state specified at $T_L = 0.60T_{\rm cri}^V$, $0.64T_{\rm cri}^V$, and $0.68T_{\rm cri}^V$; (b) density fields, (c) velocity fields, and (d) temperature fields obtained from Boltzmann equation (DSMC method) and Enskog–Vlasov equation (EVDSMC method).

simplicity. However, the dependence of the NC-gas number density on these coefficients will not change significantly even if vapor and NC gas molecules become other molecules. In future work, we will investigate these coefficients for a realistic molecular model using the results of the present study. Additionally, as a relatively weak non-equilibrium state was assumed in this study because ΔT_L is not considerably large, we will investigate vapor condensation under strong non-equilibrium conditions, e.g., for the final stage of a collapsing vapor bubble containing NC-gas molecules.

ACKNOWLEDGMENTS

This work was supported by JSPS KAKENHI Grant No. JP20K04277 (K.K.).

AUTHOR DECLARATIONS

Conflict of Interest

The authors have no conflicts to disclose.

DATA AVAILABILITY

The data that support the findings of this study are available from the corresponding author upon reasonable request.

REFERENCES

[1]C. Cercignani, *Rarefied Gas Dynamics: From Basic Concepts to Actual Calculations* (Cambridge University Press, 2000).
[2]Y. Sone, *Molecular Gas Dynamics* (Birkhäuser, 2007).
[3]D. N. Gerasimov and E. I. Yurin, *Kinetics of Evaporation* (Springer, 2018).
[4]Y. B. Zudin, *Non-Equilibrium Evaporation and Condensation Processes: Analytical Solutions* (Springer Nature, 2019).
[5]S. Takata and K. Aoki, "Two-surface problems of a multicomponent mixture of vapors and noncondensable gases in the continuum limit in the light of kinetic theory," Phys. Fluids **11**, 2743–2756 (1999).
[6]A. P. Kryukov, V. Y. Levashov, and I. N. Shishkova, "Evaporation in mixture of vapor and gas mixture," Int. J. Heat Mass Transfer **52**, 5585–5590 (2009).
[7]S. Taguchi, K. Aoki, and S. Takata, "Vapor flows condensing at incidence onto a plane condensed phase in the presence of a noncondensable gas. I. Subsonic condensation," Phys. Fluids **15**, 689–705 (2003).
[8]R. Marek and J. Straub, "Analysis of the evaporation coefficient and the condensation coefficient of water," Int. J. Heat Mass Transfer **44**, 39–53 (2001).
[9]M. Bond and H. Struchtrup, "Mean evaporation and condensation coefficients based on energy dependent condensation probability," Phys. Rev. E **70**, 061605 (2004).
[10]A. H. Persad and C. A. Ward, "Expressions for the evaporation and condensation coefficients in the Hertz-Knudsen relation," Chem. Rev. **116**, 7727–7767 (2016).
[11]R. Meland, A. Frezzotti, T. Ytrehus, and B. Hafskjold, "Nonequilibrium molecular-dynamics simulation of net evaporation and net condensation, and

evaluation of the gas-kinetic boundary condition at the interphase," Phys. Fluids **16**, 223–243 (2004).
[12]T. Ishiyama, T. Yano, and S. Fujikawa, "Molecular dynamics study of kinetic boundary condition at an interface between argon vapor and its condensed phase," Phys. Fluids **16**, 2899–2906 (2004).
[13]T. Ishiyama, T. Yano, and S. Fujikawa, "Kinetic boundary condition at a vapor-liquid interface," Phys. Rev. Lett. **95**, 084504 (2005).
[14]K. Kobayashi, K. Hori, M. Kon, K. Sasaki, and M. Watanabe, "Molecular dynamics study on evaporation and reflection of monatomic molecules to construct kinetic boundary condition in vapor-liquid equilibria," Heat Mass Transfer **52**, 1851–1859 (2016).
[15]V. V. Zhakhovsky, A. P. Kryukov, V. Y. Levashov, I. N. Shishkova, and S. I. Anisimov, "Mass and heat transfer between evaporation and condensation surfaces: Atomistic simulation and solution of Boltzmann kinetic equation," Proc. Natl. Acad. Sci. **116**, 18209–18217 (2019).
[16]A. Tokunaga and T. Tsuruta, "Nonequilibrium molecular dynamics study on energy accommodation coefficient on condensing liquid surface–molecular boundary conditions for heat and mass transfer," Phys. Fluids **32**, 112011 (2020).
[17]A. Frezzotti, L. Gibelli, and S. Lorenzani, "Mean field kinetic theory description of evaporation of a fluid into vacuum," Phys. Fluids **17**, 012102 (2005).
[18]K. Kobayashi, K. Ohashi, and M. Watanabe, "Numerical analysis of vapor-liquid two-phase system based on the Enskog-Vlasov equation," AIP Conf. Proc. **1501**, 1145–1151 (2012).
[19]M. Kon, K. Kobayashi, and M. Watanabe, "Method of determining kinetic boundary conditions in net evaporation/condensation," Phys. Fluids **26**, 072003 (2014).
[20]M. Kon, K. Kobayashi, and M. Watanabe, "Liquid temperature dependence of kinetic boundary condition at vapor-liquid interface," Int. J. Heat Mass Transfer **99**, 317–326 (2016).
[21]M. Kon, K. Kobayashi, and M. Watanabe, "Kinetic boundary condition in vapor-liquid two-phase system during unsteady net evaporation/condensation," Eur. J. Mech. B. Fluids **64**, 81–92 (2017).
[22]A. Frezzotti, "Non-equilibrium structure of the vapor-liquid interface of a binary fluid," AIP Conf. Proc. **1333**, 161–166 (2011).
[23]K. Kobayashi, K. Sasaki, M. Kon, H. Fujii, and M. Watanabe, "Kinetic boundary conditions for vapor–gas binary mixture," Microfluid. Nanofluid. **21**, 53 (2017).
[24]K. Ohashi, K. Kobayashi, H. Fujii, and M. Watanabe, "Evaporation coefficient and condensation coefficient of vapor under high gas pressure conditions," Sci. Rep. **10**, 8143 (2020).
[25]K. Kobayashi, T. Nagayama, M. Watanabe, H. Fujii, and M. Kon, "Molecular gas dynamics analysis on condensation coefficient of vapour during gas–vapour bubble collapse," J. Fluid Mech. **856**, 1045–1063 (2018).
[26]Y. Onishi, "The spherical-droplet problem of evaporation and condensation in a vapour-gas mixture," J. Fluid Mech. **163**, 171–194 (1986).
[27]S. Fujikawa, T. Yano, and M. Watanabe, *Vapor-Liquid Interfaces, Bubbles and Droplets: Fundamentals and Applications* (Springer Science and Business Media, 2011).
[28]J. Karkheck and G. Stell, "Mean field kinetic theories," J. Chem. Phys. **75**, 1475 (1981).
[29]A. Frezzotti, L. Gibelli, D. A. Lockerby, and J. E. Sprittles, "Mean-field kinetic theory approach to evaporation of a binary liquid into vacuum," Phys. Rev. Fluids **3**, 054001 (2018).
[30]P. Resibois and M. De Leener, *Classical Kinetic Theory of Fluids* (Wiley, 1977).
[31]A. Frezzotti, "A particle scheme for the numerical solution of the Enskog equation," Phys. Fluids **9**, 1329–1335 (1997).
[32]E. S. Benilov and M. S. Benilov, "Energy conservation and H theorem for the Enskog-Vlasov equation," Phys. Rev. E **97**, 062115 (2018).
[33]K. Aoki, S. Takata, and S. Kosuge, "Vapor flows caused by evaporation and condensation on two parallel plane surfaces: Effect of the presence of a non-condensable gas," Phys. Fluids **10**, 1519–1533 (1998).
[34]A. Frezzotti, P. Barbante, and L. Gibelli, "Direct simulation Monte Carlo applications to liquid-vapor flows," Phys. Fluids **31**, 062103 (2019).
[35]S. Busuioc, L. Gibelli, D. A. Lockerby, and J. E. Sprittles, "Velocity distribution function of spontaneously evaporating atoms," Phys. Rev. Fluids **5**, 103401 (2020).
[36]A. Frezzotti and P. Barbante, "Kinetic theory aspects of non-equilibrium liquid-vapor flows," Mech. Eng. Rev. **4**, 16-00540 (2017).
[37]Y. P. Pao, "Application of kinetic theory to the problem of evaporation and condensation," Phys. Fluids **14**, 306–312 (1971).
[38]L. D. Koffman, M. S. Plesset, and L. Lees, "Theory of evaporation and condensation," Phys. Fluids **27**, 876–880 (1984).
[39]J. C. Haas and G. S. Springer, "Mass transfer through binary gas mixtures," J. Heat Transfer **95**, 263–265 (1973).
[40]T. Soga, "Kinetic analysis of evaporation and condensation in a vapor–gas mixture," Phys. Fluids **25**, 1978–1986 (1982).
[41]K. Gu, C. B. Watkins, and J. Koplik, "Molecular dynamics simulation of the equilibrium liquid–vapor interphase with solidification," Fluid Phase Equilib. **297**, 77–89 (2010).
[42]H. Tabe, K. Kobayashi, H. Fujii, and M. Watanabe, "Molecular dynamics study on characteristics of reflection and condensation molecules at vapor-liquid equilibrium state," PLOS One **16**, e0248660 (2021).
[43]R. Meland, "Molecular dynamics simulation of the inverted temperature gradient phenomenon," Phys. Fluids **15**, 3244–3247 (2003).
[44]M. P. Allen and D. J. Tildesley, *Computer Simulation of Liquids* (Oxford, 1987).
[45]M. Kon, "Mean-field kinetic theory based study of boundary condition at vapor-liquid interface," Ph.D. thesis (Hokkaido University, 2017).
[46]G. A. Bird, *Molecular Gas Dynamics and the Direct Simulation of Gas Flows* (Clarendon Press, Oxford, 1994).